Supporting Information

A New Selection Criterion for Potential Window of Aqueous Zinc Ion Hybrid Capacitors: Achieving a Balance Between Energy Density and Cycle Stability

Fanda Zeng[a], Xiliang Gong[a], Zijin Xu[a], Zhengyan Du[a], Jian Xu[a], Ting Deng[a], Dong Wang[a], Yi Zeng[a], Shansheng Yu[a], Zeshuo Meng*[,a], Xiaoying Hu*[,b], Hongwei Tian*[,a]

[a] Key Laboratory of Automobile Materials of MOE and School of Materials Science and Engineering, Jilin University, Changchun, 130012, China

[b] College of Science and Laboratory of Materials Design and Quantum Simulation, Changchun University, Changchun, 130022, China

*Corresponding Authors: Z. S. Meng: mengzs21@mails.jlu.edu.cn; X. Y. Hu: huxy@ccu.edu.cn; H.W. Tian: tianhw@jlu.edu.cn.

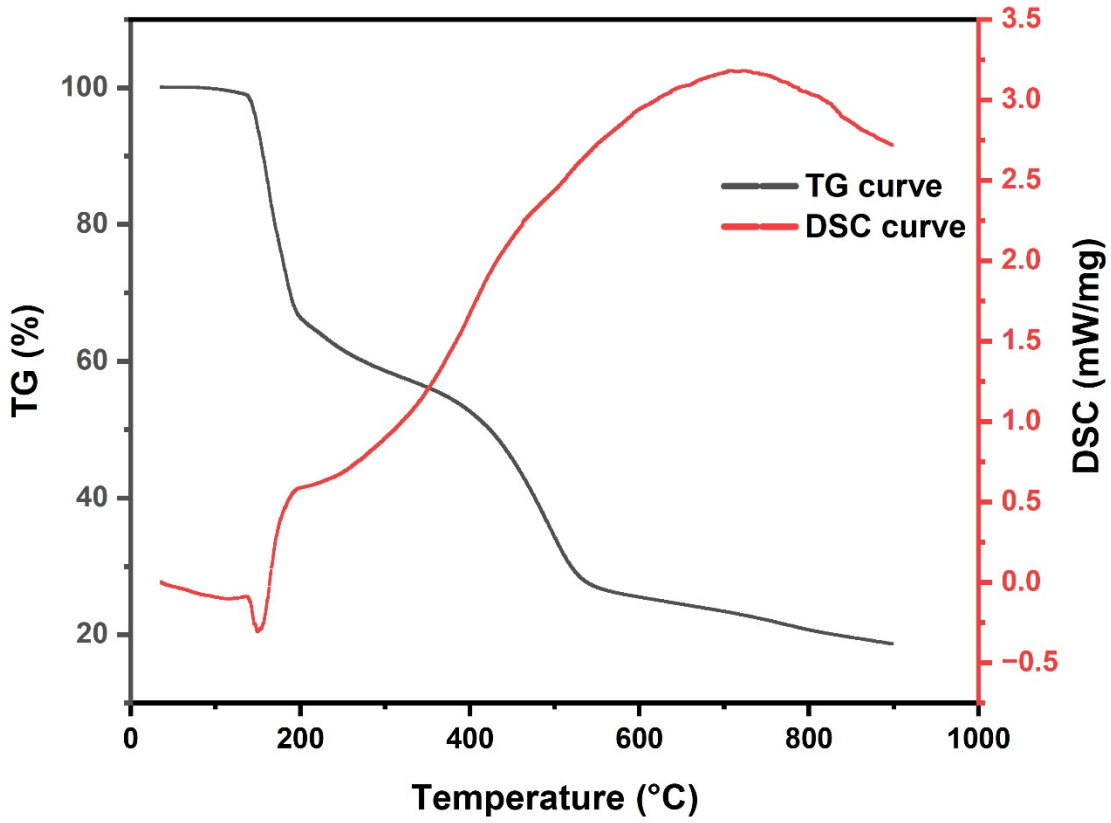

Figure S1 TGA and DSC test of a mixture of 1 g glucose and 0.5 g $ZnCl_2$ from 0℃ to 900℃

TGA and DSC test was conducted to reveal the activation process of glucose during annealing. As it shown in **Figure S1**, according to the TGA curve, the glucose had two obvious mass loss stages, which meant that it was dehydrated and carbonized during this process. Besides, the DSC curve showed a heat absorption peak that started at 141℃, and ended at 172℃, it revealed the melting process of glucose. As a result, it can be illustrated by combining the TGA and DSC curves that the molten state and vaporization process of zinc chloride etched glucose, resulting in ultrathin carbon materials.

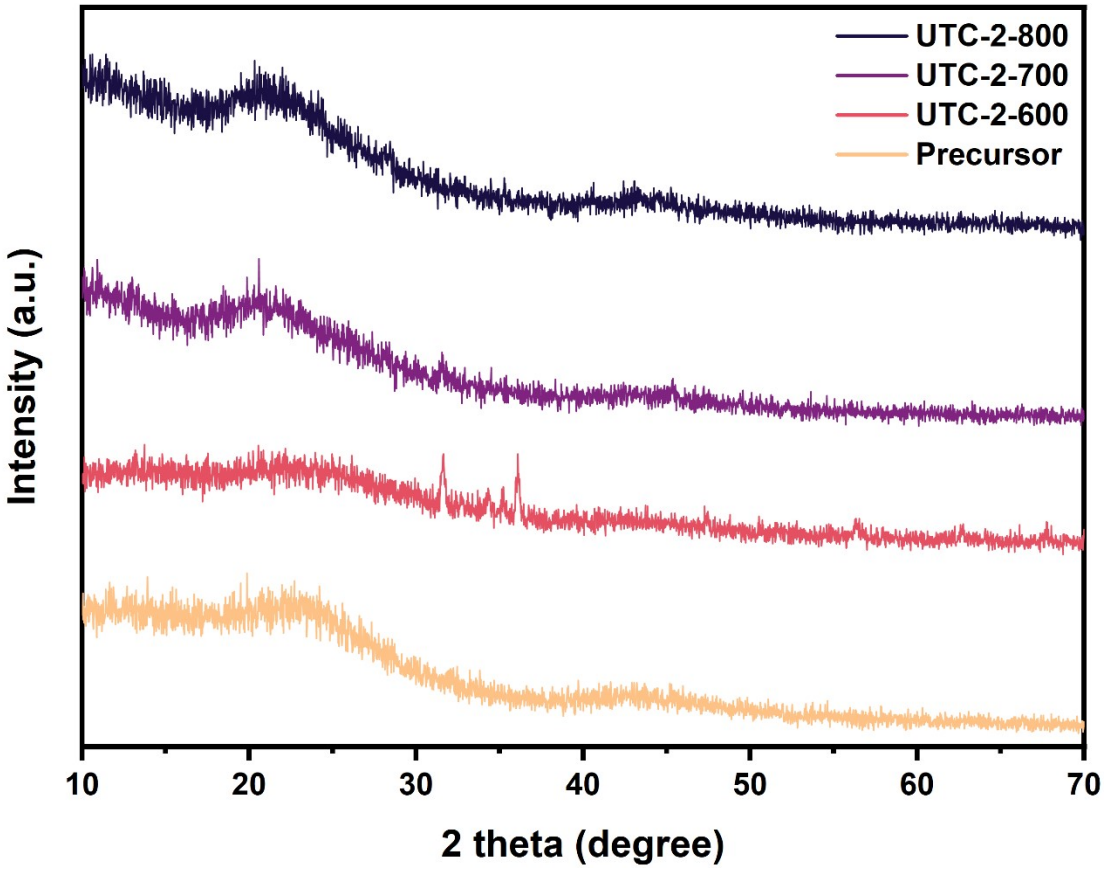

Figure S2 XRD patterns of UTCs and precursor.

The X-ray diffraction (XRD) patterns (**Figure S2**) of UTC-2-700, UTC-800 and precursor showed two broad peaks at 22.2° and 43.1°, assigning to the (002) and (100) planes of graphitic carbon, respectively. However, the XRD pattern of UTC-2-600 showed more peaks, which was attributed to the incomplete vaporization of zinc chloride.

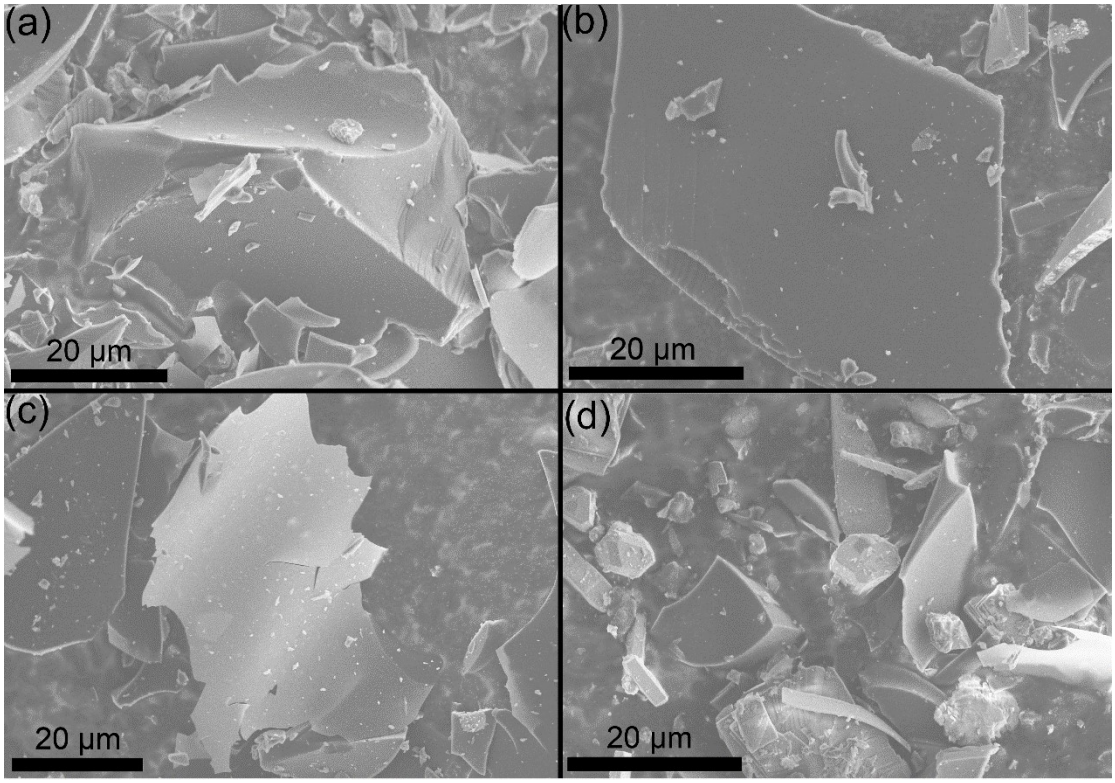

Figure S3 SEM images of (a) precursor, (b) UTC-2-600, (c) UTC-2-700, (d) UTC-2-800

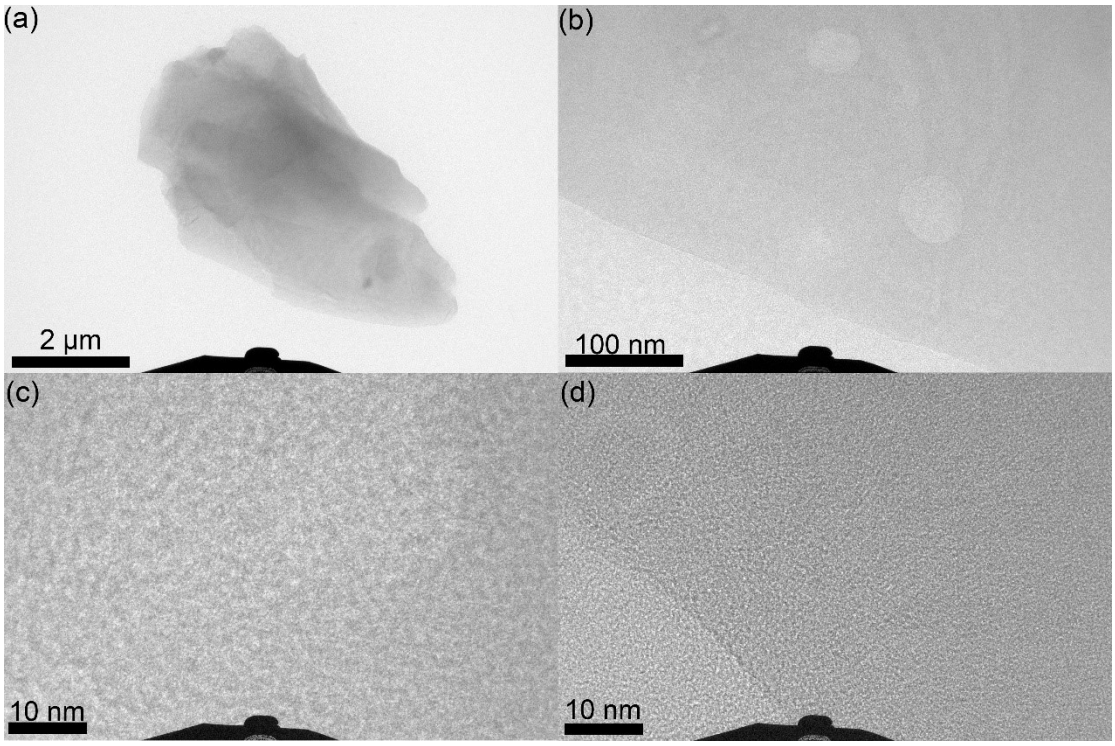

Figure S4 TEM images of UTC-2-700.

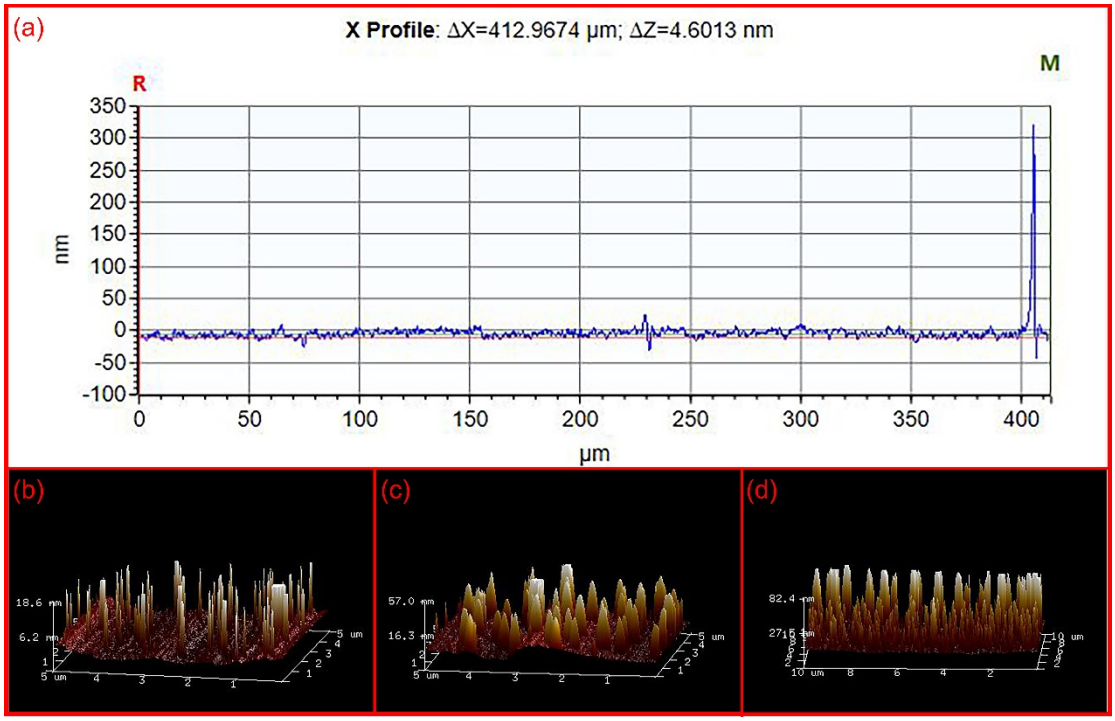

Figure S5 (a) White light Interference microscope test of precursor, AFM test of (b) UTC-2-700, (c) UTC-2-600, (d) UTC-2-800.

According to image of White light Interference microscope test, average thickness of precursor is about 410 nm. However, the maximum thickness of UTCs is less than 100 nm, which demonstrates the effective etching of $ZnCl_2$. To be specific, the thinnest thickness of UTC-2-700 is 4.78 nm, which is almost one hundredth the thickness of the precursor.

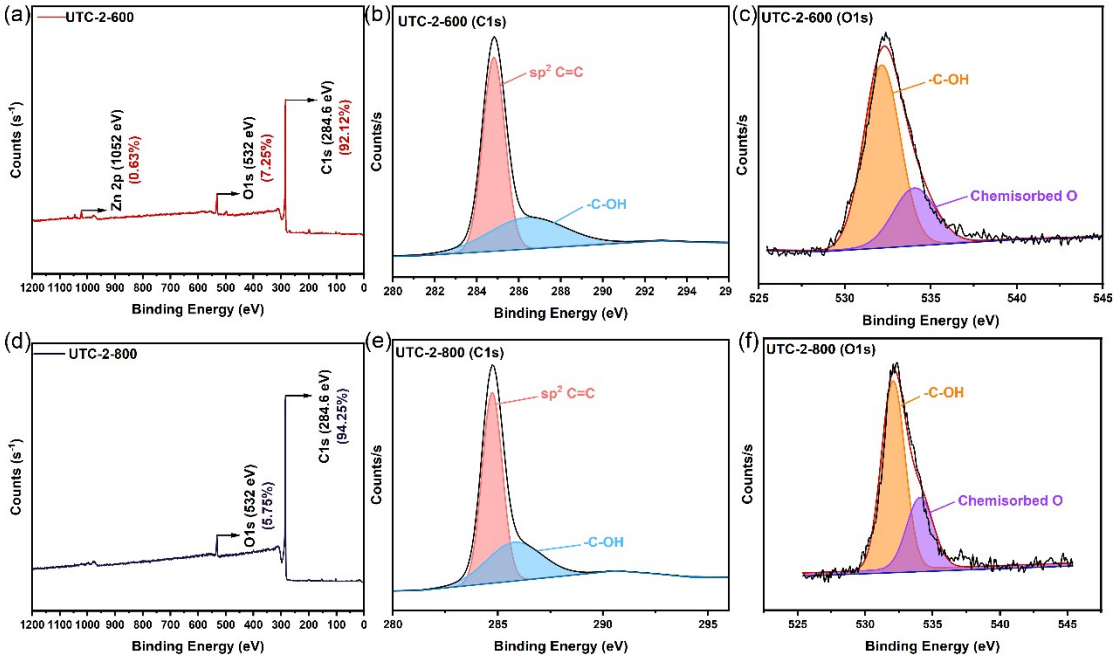

Figure S6 (a) XPS full spectra of UTC-2-600. (b) C 1s XPS spectra of UTC-2-600. (c) O 1s XPS spectra of UTC-2-600. (d) XPS full spectra of UTC-2-800. (e) C 1s XPS spectra of UTC-2-800. (f) (b) O 1s XPS spectra of UTC-2-800.

The XPS full spectrum analysis shows that there are still residual Zn elements in UTC-2-600, which is due to incomplete vaporization of $ZnCl_2$. Due to inadequate and overactivation, the oxygen content of UTC-2-600 and UTC-2-800 were not significantly increased compared to precursor (**Figure S6 (a) and (d)** and **Figure 1(e)**). However, compared with precursor, the relative proportion of -C-OH of UTC-2-600 and UTC-2-800 (**Figure S6 (c) and (f)**) is higher than precursor (**Figure 1(f)**).

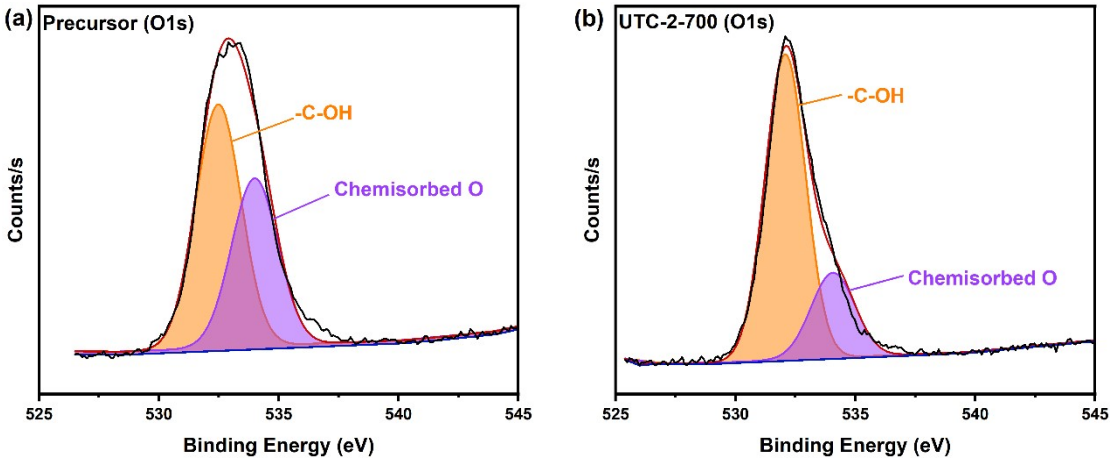

Figure S7 (a) O 1s XPS spectra of precursor. (b) O 1s XPS spectra of UTC-2-700.

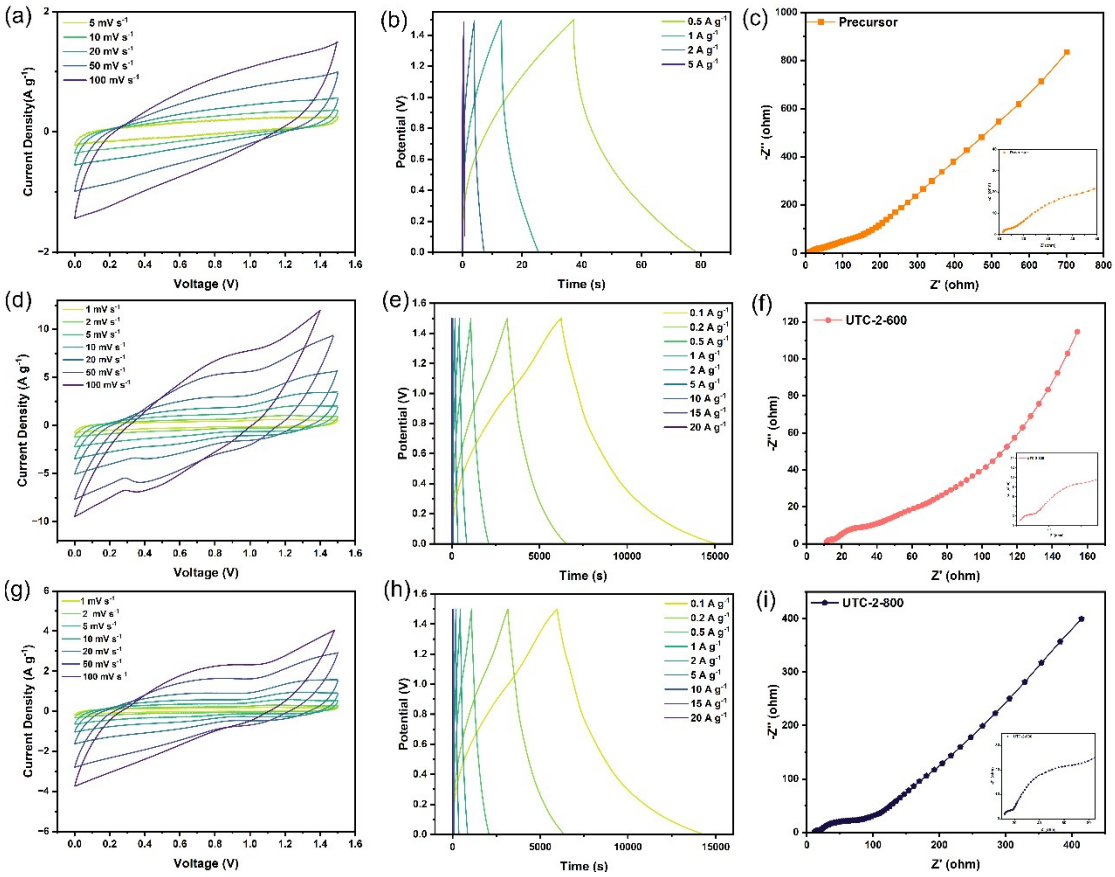

Figure S8. The voltage window for electrochemical testing was 1.5 V in 1M $ZnSO_4$ electrolyte. (a) CV curves of precursor. (b) GCD curves of precursor. (c) EIS curve of precursor. (d) CV curves of UTC-2-600. (e) GCD curves of UTC-2-600. (f) EIS curve of UTC-2-600. (g) CV curves of UTC-2-800. (h) GCD curves of UTC-2-800. (i) EIS curve of UTC-2-800.

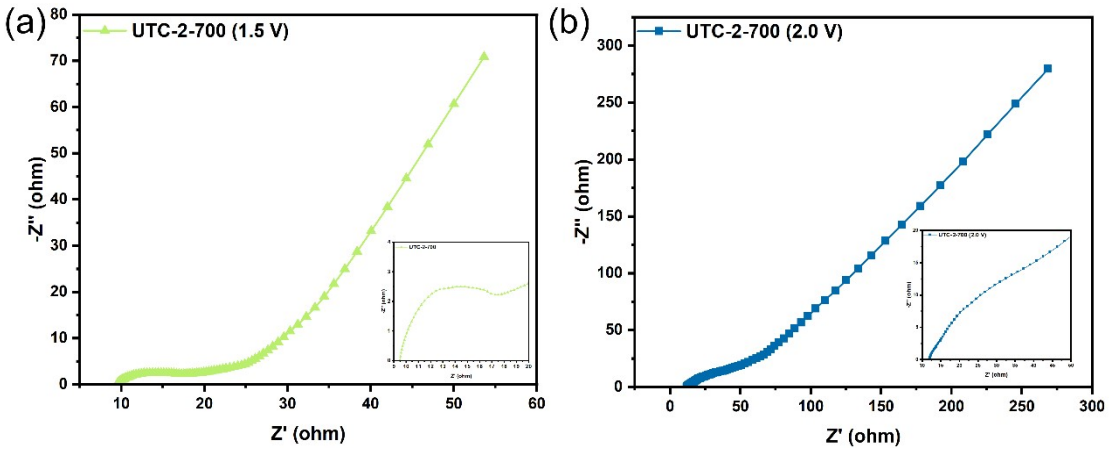

Figure S9. EIS curve of UTC-2-700 in 1M $ZnSO_4$ electrolyte at (a) 0-1.5 V, (b)0-2.0 V.

It can be seen from **Figure S9(a) and (b)** that UTC-2-700 displays smaller charge-transfer resistance (R_{ct}) at 1.5 V, suggesting the fast charge transfer and good electrode/electrolyte interface. The excellent electrode/electrolyte interface is attributed to the favorable electrolyte infiltration and luxuriant oxygen doping. More importantly, since the surface of UTC-2-700 was destroyed at 2.0 V, the surface group content was lower, resulting in higher R_{ct} and worse ion transport.

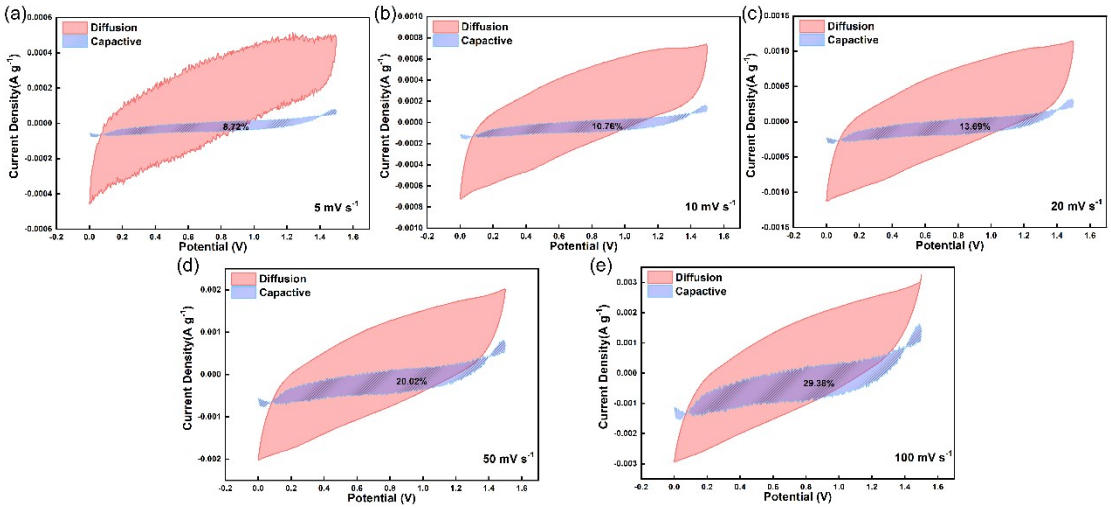

Figure S10. Ultrarapid reaction kinetics contribution at different scan rates of precursor.

To further study the enhanced electrochemical capability and charge-storage contribution of precursor, UTC-2-700-1.5 V and UTC-2-700-2.0 V, CV curves at various scan rates from 5 to 100 mV s^{-1} were systematically analyzed. The relationship between peak current (i) and scan rate (v) can be shown as following equation

$$i = av^b \quad (1)$$

where a and b are variable constants, and the b value can be obtained by fitting the relationship curve between log(i) and log(v). When the b value is 0.5 and 1, corresponds sluggish reaction kinetics and capacitive behavior-dominated ultrarapid reaction kinetics, respectively.[1, 2]

Besides, since each electrochemical reaction can be regarded as a combination of capacitive behavior-dominated and diffusion-controlled process, the total current (i) of the electrochemical reaction can be divided by capacitive behavior-dominated and diffusion-controlled contribution like the following equation:

$$i = k_1 v + k_2 v^{1/2} \quad (2)$$

where i represents total current, k_1v and $k_2v^{1/2}$ represent the current contributed by capacitive behavior-dominated process and diffusion-controlled process, respectively.[3]

It can be seen from **Figure S11, S12 and S13** that with increasing scan rate, the charge capacity stored through diffusion-controlled process decreases, indicating the capacitive contribution ratios of capacitive process is enhanced with the elevation of the scan rate[4]. But the high percentages of their capacity still originate from diffusion-controlled process with relatively slow charge storage kinetics, suggesting their high capacity and inferior rate capability.

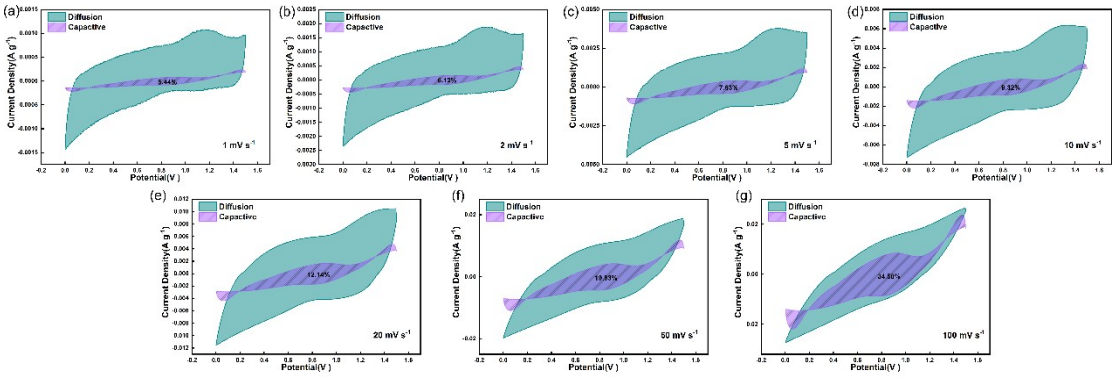

Figure S11. Ultrarapid reaction kinetics contribution at different scan rates of UTC-2-700 at 0-1.5 V.

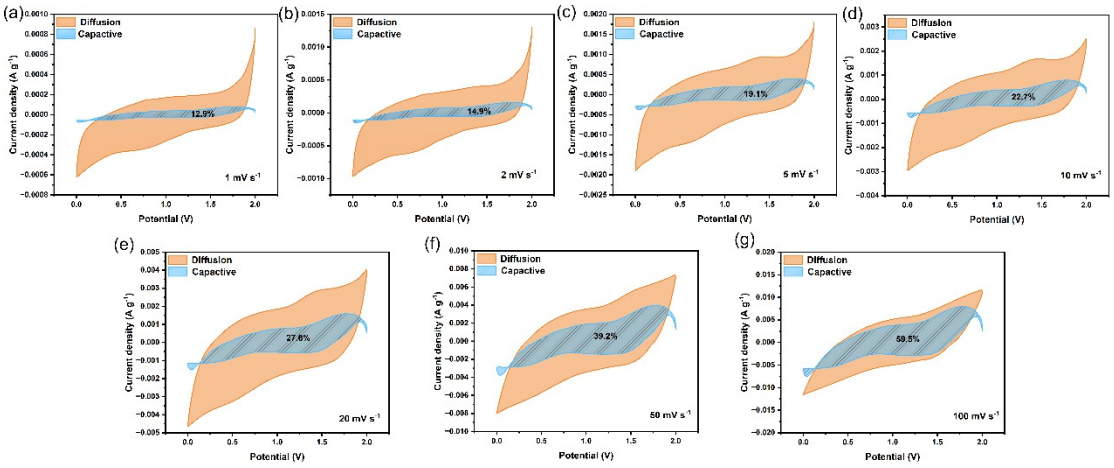

Figure S12. Ultrarapid reaction kinetics contribution at different scan rates of UTC-2-700 at 0-2.0 V.

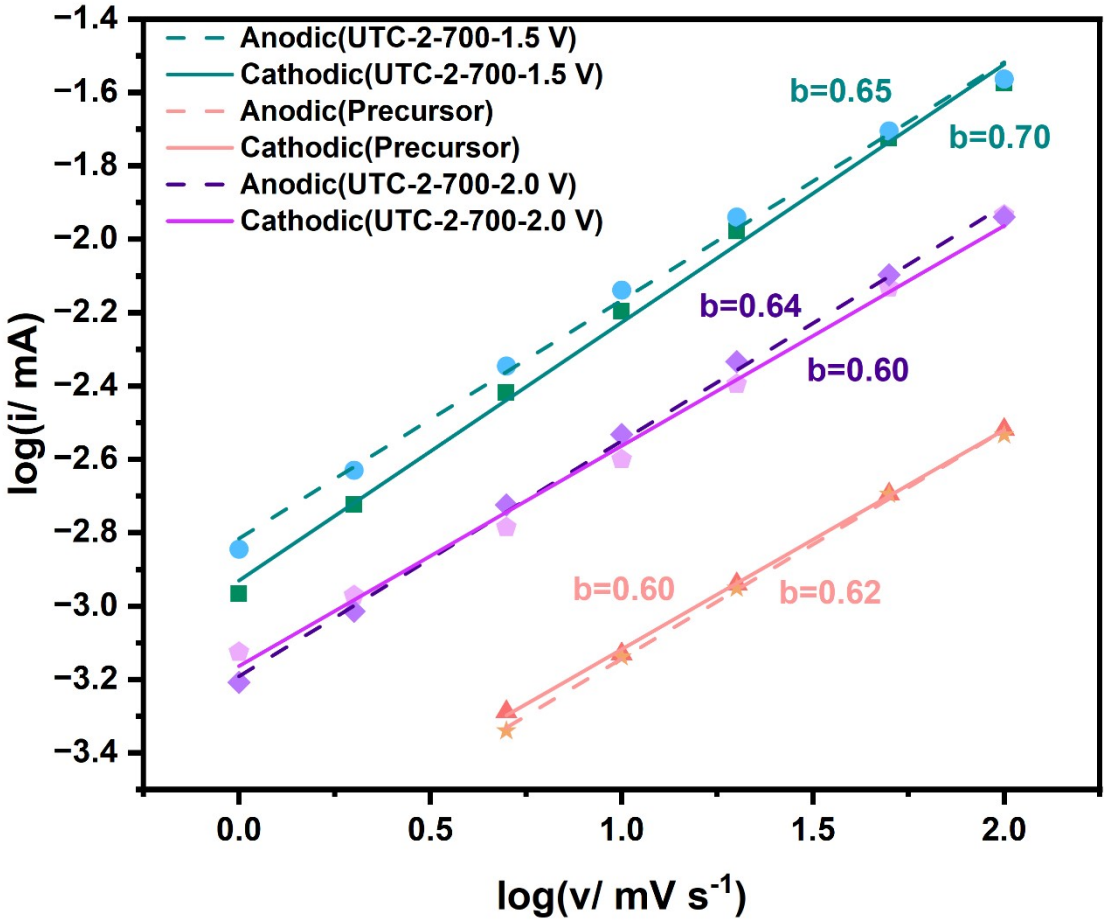

Figure S13. Linear relationships between logarithm currents and logarithm sweep rate of precursor, UTC-2-700 at 0-1.5 V, and UTC-2-700 at 0-2.0 V.

By contrast, as depicted in **Figure S14**, b value of the Anodic of UTC-2-700-1.5 V is close to UTC-2-700-2.0 V, while b value of the cathodic of UTC-2-700-1.5 V is higher than that of UTC-2-700-2.0 V, which means UTC-2-700-1.5 V possesses high capacity contribution ratios of capacitive process and fast charge storage kinetics[4]. Therefore, this phenomenon can prove that the decrease in cycling stability is caused by cathode destruction.

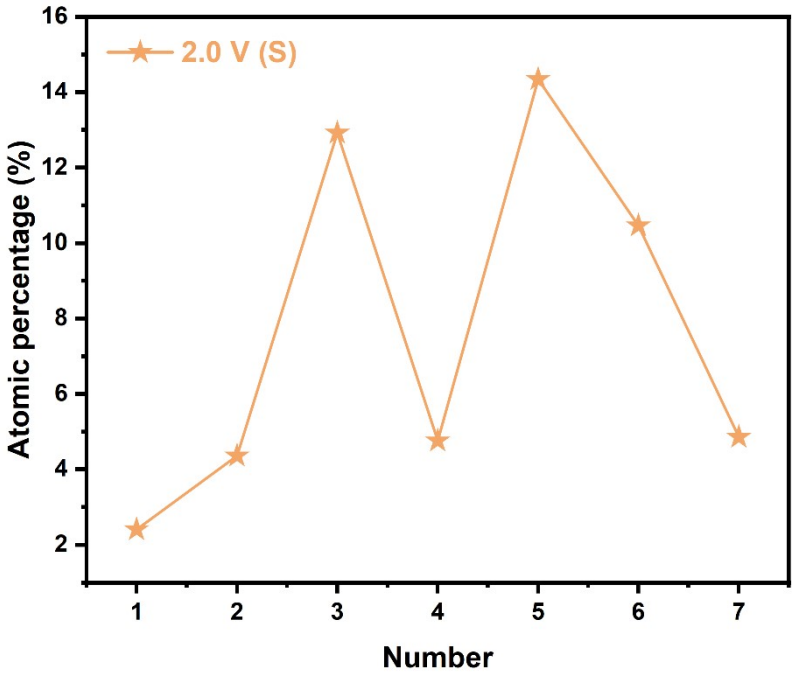

Figure S14. In the process of charge and discharge, the content of sulfur element on the surface of the material at different voltages due to XPS test.

The content of sulfur had the same change trend as that of zinc, and it is also demonstrated that basic zinc sulfate is destroyed at 2.0 V.

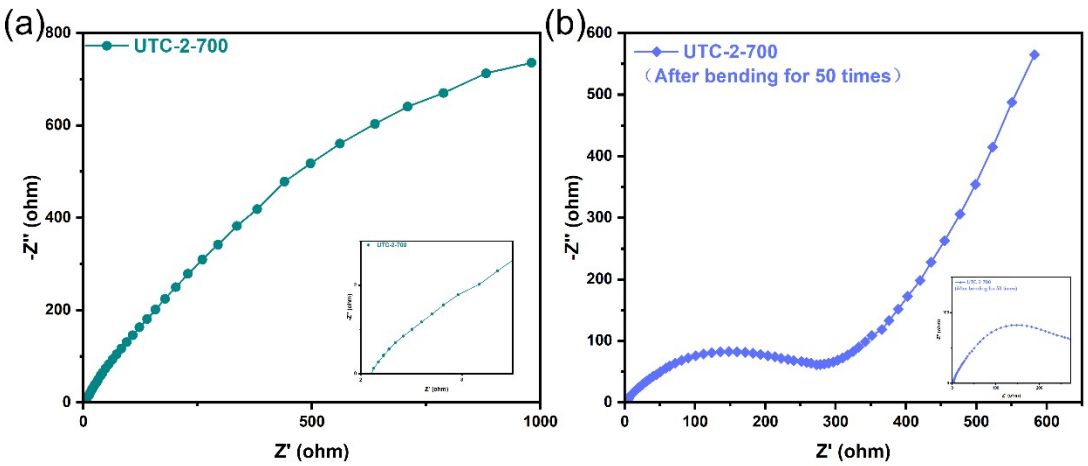

Figure S15. (a) EIS curve of a flat pouch cell prepared with UTC-2-700 (b) EIS curve of a flat pouch cell prepared with UTC-2-700 after being folded up to 180° for 50 times.

By comparison, it is obvious that the R_{ct} of the flat pouch cell was increased after multiple folds, which is mainly caused by the bending of the zinc sheet and the stainless steel mesh that causes the electron transport to be blocked.[5]

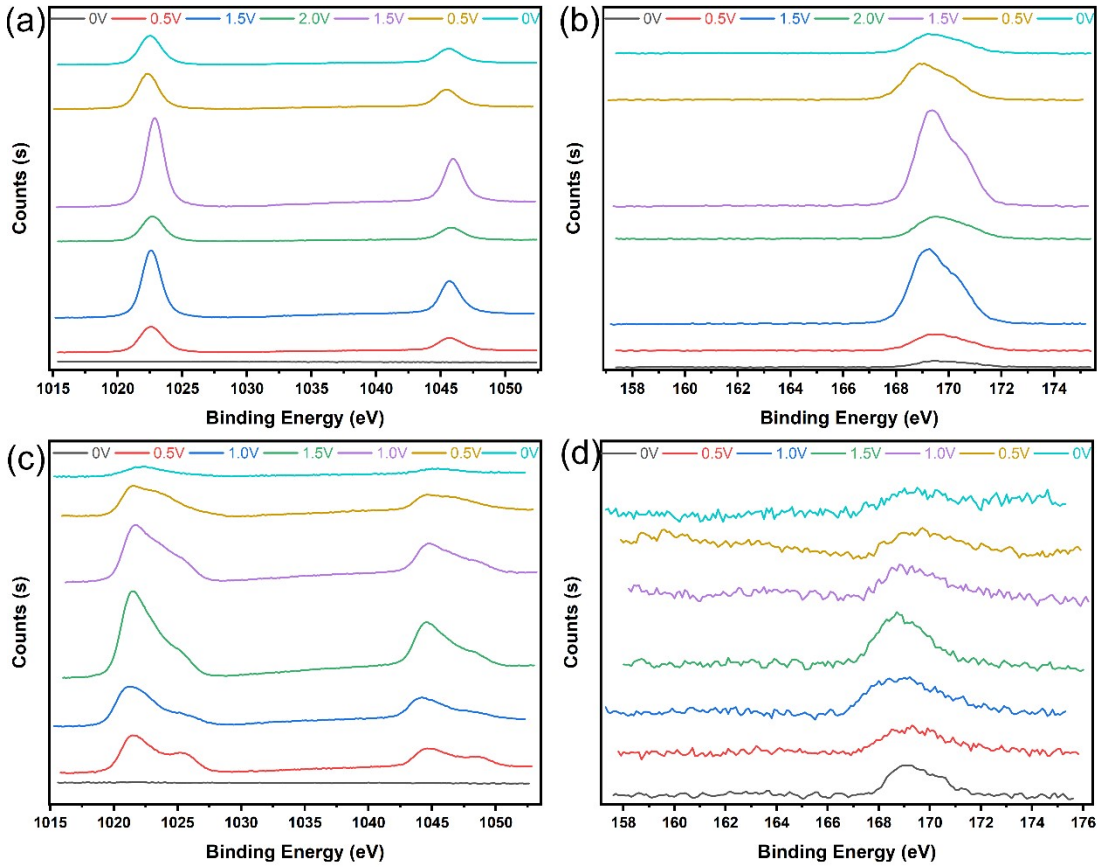

Figure S16. (a)XPS spectra of Zn 2p from 0 V-2.0 V (b) XPS spectra of S 2p from 0 V-2.0 V(c) XPS spectra of Zn 2p from 0 V-1.5 V(d) XPS spectra of S 2p from 0 V-1.5 V

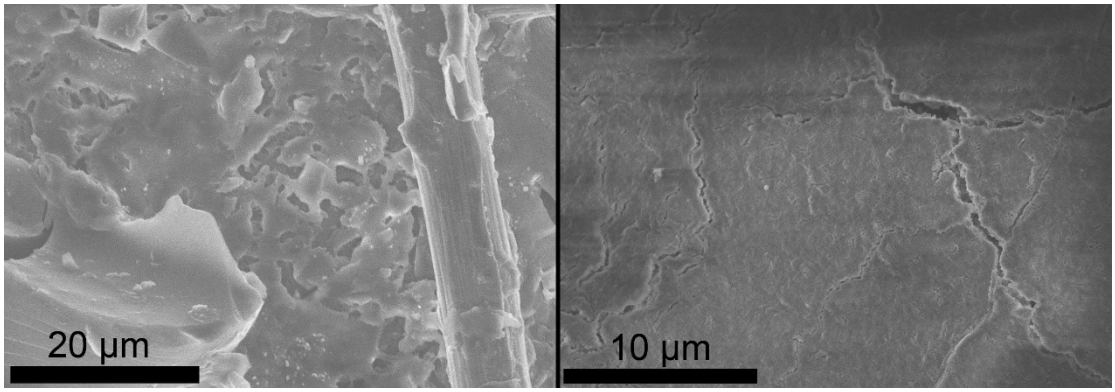

Figure S17. (a)SEM image of UTC-2-700 coated on carbon paper (before testing). (b) SEM image of UTC-2-700 coated on carbon paper (after 3000 cycles)

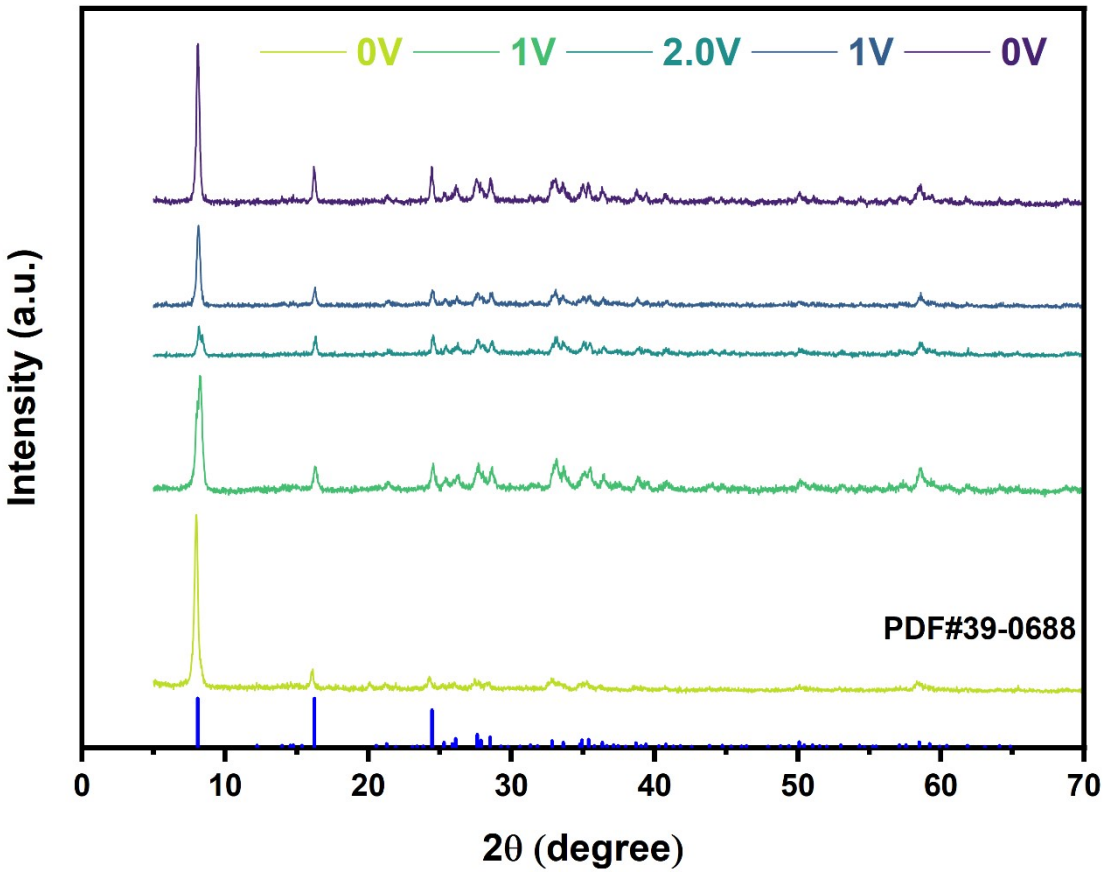

Figure S18. XRD diffractograms of cathode surface byproducts ($Zn_4SO_4(OH)_6 \cdot 5H_2O$) at different voltages during charging and discharging processes.

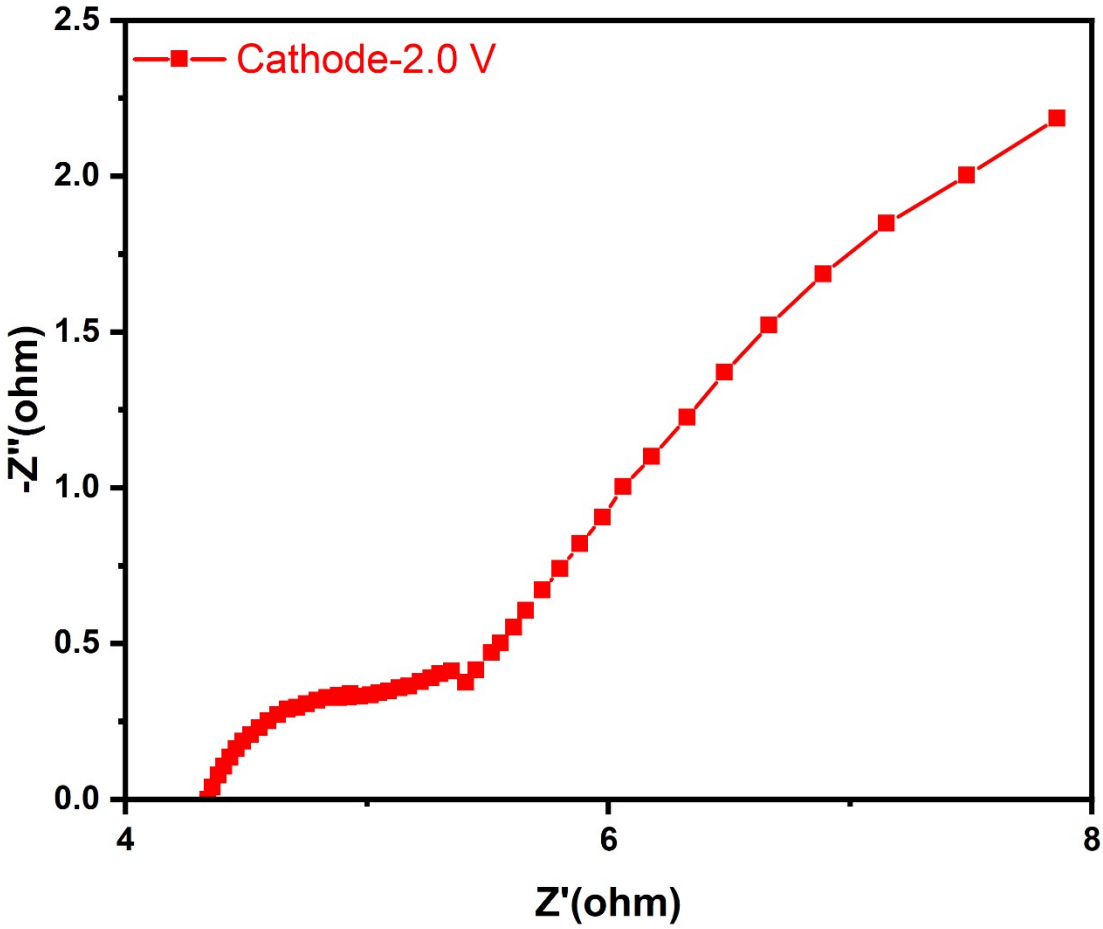

Figure S19. EIS image of a zinc anode

The value of R_s is calculated to be 4.361 and the value of R_{ct} is 0.608, which is small compared to the total capacitor resistance in Table S3, and it can be assumed that the overall EIS test results are representative of the cathode test results

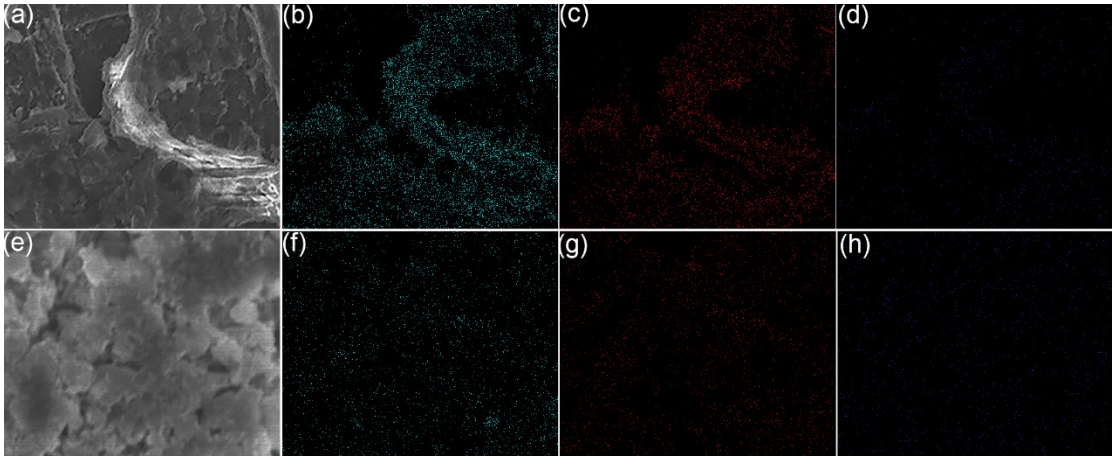

Figure S20. SEM images of complete basic zinc sulfate layer (a) and broken basic zinc sulfate layer (b) EDS mapping images of Zn((b) and (f)) O((c) and (g))and S((d) and (h)) elements on UTC-2-700 surface.

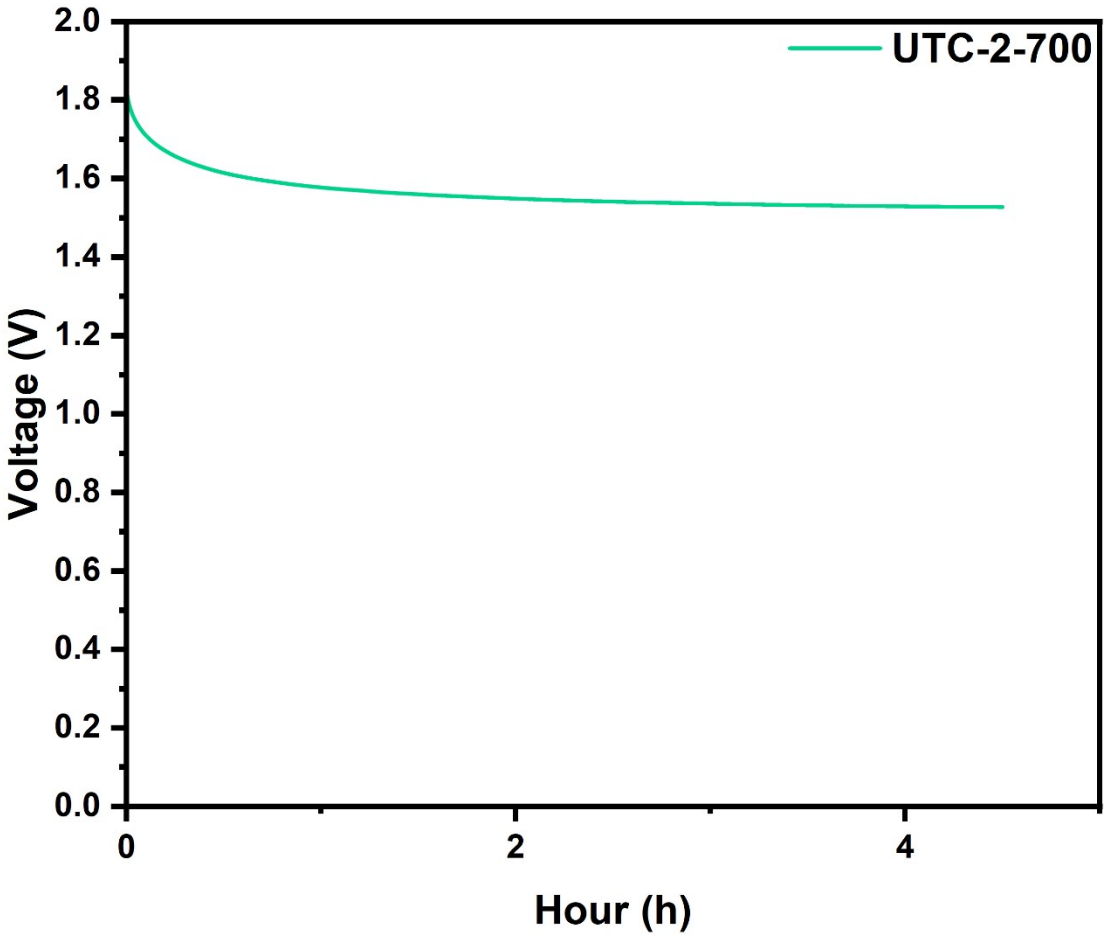

Figure S21 IR loss of the flat pouch ZHSs. An flat pouch ZHS was charged/discharged through GCD technique at 0.1 A g^{-1} for 3 cycles and then maintained at an expected voltage using constant voltage charging technique for 30 min. This is to make internal environment of the electrochemical device reaches a relatively stable state.

Table S1 BET test of precursor and UTCs.

Material	BET surface area (m^2 g^{-1})	Average pore diameter (nm)	t-Plot external surface area (cm^2 g^{-1})	t-Plot micropore volume (cm^3 g^{-1})	t-Plot micropore area(m^2g^{-1})
Precursor	274.6	1.6659	9.1	0.101232	265.5
UTC-2-600	713.4	2.1910	114.6	0.325692	598.8
UTC-2-700	952.0	2.4510	220.8	0.398680	731.2
UTC-2-800	900.3	2.1781	156.2	0.405607	744.0

Table S2 Specific capacitance at a voltage window of 1.5 V in 1M $ZnSO_4$ electrolyte in the two-electrodes system.

Specific capacitance (mAh g^{-1}) / Current density (A g^{-1}) / Materials	0.1	0.2	0.5	1	2	5	10	15	20
Precursor			5.76	3.44	1.8	0.42			
UTC-2-600	245.3	186.7	141.4	112.6	92.2	62.2	36.1	20.4	10.6
UTC-2-700	360.0	264.9	201.8	165.8	139.1	100.4	69.2	46.3	29.4
UTC-2-800	232.0	179.1	137.8	115.1	94.4	64.6	39.7	22.1	10.6

Table S3. R_s and R_{ct} values of precursor and UTCs according to EIS curves.

Material	R_s (Ω)	R_{ct} (Ω)
Precursor	11.5	10
UTC-2-600	11.29	6.18
UTC-2-700	9.485	11.815
UTC-2-800	11.99	11.4

Table S4. Specific capacity, energy density and power density at different current densities of the flat pouch cell prepared with UTC-2-700 at 0-1.9 V.

Current density ($A\ g^{-1}$)	Specific capacity ($mAh\ g^{-1}$)	Energy density ($Wh\ kg^{-1}$)	Power density ($W\ kg^{-1}$)
0.1	66.47222	119.9824	95
0.2	53.44444	96.46722	190
0.5	38.16667	68.89083	475
1	32.55556	58.76278	950
2	18.44444	33.29222	1900
5	5.833333	10.52917	4750
10	0.277778	0.501389	9500

Table S5. Performance comparison of different flexible zinc ion hybrid supercapacitors.

Device	Energy density (Wh kg^{-1})	Power density (W kg^{-1})	Reference
This work	120.0	95	
quasi-solid-state ZHCs	60.1	74.2	[6]
quasi-solid-state ZHS	27.7	35.7	[7]
FSC	11.1	250	[8]
Zn//Co/Zn-ZIF(M24)@CC ZHC	49.2	124.6	[9]
Zn//PAAm/agar/Zn(CF3SO3)2//NC			[10]
ZHSC	61.3	209.0	
quasi-solid-state Zn//NMXC	54.9	75.8	[11]

Reference

1. Q. Guo, Y. Han, N. Chen and L. Qu, *ACS Energy Lett.*, 2021, **6**, 1786-1794.
2. M. Forghani and S. W. Donne, *J. Electrochem. Soc.*, 2019, **166**, A1370-A1379.
3. L. Dong, W. Yang, W. Yang, C. Wang, Y. Li, C. Xu, S. Wan, F. He, F. Kang and G. Wang, *Nano-Micro Lett.*, 2019, **11**, 94.
4. L. Wang, M. Peng, J. Chen, X. Tang, L. Li, T. Hu, K. Yuan and Y. Chen, *ACS Nano*, 2022, **16**, 2877-2888.
5. H. Tang, J. Yao and Y. Zhu, *Adv. Energy Mater.*, 2021, **11**, 2003994.
6. F. Wei, Y. Wei, J. Wang, M. Han and Y. Lv, *Chem. Eng. J.*, 2022, **450**, 137919.
7. G. Lou, G. Pei, Y. Wu, Y. Lu, Y. Wu, X. Zhu, Y. Pang, Z. Shen, Q. Wu, S. Fu and H. Chen, *Chem. Eng. J.*, 2021, **413**, 127502.
8. Y. Li, W. Ou-Yang, X. Xu, M. Wang, S. Hou, T. Lu, Y. Yao and L. Pan, *Electrochim. Acta*, 2018, **271**, 591-598.
9. X. Chen, Y. Li, L. Li, Q. Zhu, B. Liang, J. Zhao and W. Zhang, *Scr. Mater.*, 2023, **225**, 115171.
10. W. Xie, W. Yang, P. Xie and W. Xie, *J. Electrochem. Soc.*, 2022, **169**, 110539.
11. H. Cui, H. Mi, C. Ji, F. Guo, Y. Chen, D. Wu, J. Qiu and H. Xie, *J. Mater. Chem. A*, 2021, **9**, 23941-23954.